UWB Geo-Regioning in Rich Multipath Environment

Frank Althaus, Florian Troesch and Armin Wittneben
Communication Technology Laboratory, ETHZ, CH-8092 Zuerich
Telephone: +41 1 632 6918, Fax: +41 1 632 1209
Email: {althaus, troeschf, wittneben}@nari.ee.ethz.ch

***Abstract*— We introduce *geo-regioning* as a method to achieve rough localization in asynchronous UWB networks. The approach is to localize the transmitter position by means of the multipath components in the received channel impulse response (signature). To show the principle feasibility of this approach a first regioning algorithm is introduced and tested with measured data. Therefore, a measurement campaign in a rich multipath environment has been performed. A high number of signatures originating from different regions in a room have been collected. The regioning algorithm presented here is based on the a priori knowledge of the average power delay profiles of the different regions. The performance results show that almost all regions can be localized at reasonable SNR and error probability. We conclude that the geo-regioning approach is a promising alternative or supplement to classical time of arrival based approaches in UWB networks.**

I. Introduction

One of the most cited advantages of Ultra-Wideband (UWB) technology is the capability of performing accurate localization. The huge bandwidth introduces a very high temporal multipath resolution to the propagation channel including an accurate representation of the initial delay. Therefore, most localization and ranging approaches in UWB are based on *Time-of-Arrival* (ToA) estimation. In typical *Line-of-Sight* (LOS) conditions the first path (initial delay) is the strongest path and corresponds to the LOS component. However, if the first path does not correspond to the strongest path, more sophisticated algorithms are required to achieve an accurate estimate of the initial delay [1]. A general problem of the ToA approach is that the performance of localization/ranging systems decreases very fast in non-LOS (NLOS) conditions since here the first arriving path may not correspond to the direct path and includes an additional detouring delay [2].

In this work, we will follow a different approach exploiting the nature of UWB channels to achieve a rough localization for some specific applications. We suppose that the channel impulse response (CIR) of a transmitter/receiver (TX/RX) pair is almost unique, given by many resolvable multipath components that result from the individual geographical constellation of RX and TX. At a certain RX the CIR received from any TX is like a signature of the TX position. If two TXs have a very similar signature they are likely very close together. Although it has been shown, that the spatial correlation of the signatures strongly decreases within about 10 cm [3], we will see that there remains enough information to decide whether two signatures belong to the same geographical region or not. We refer to this approach as "geo-regioning". We assume that a region can have a size of several dm^3 up to several m^3. In data aided geo-regioning the position of some specific reference nodes in the network is known. This information is used to derive the position location information of all received signals by means of an appropriate regioning process. This facilitates a variety of location aware services and protocols in dense ad hoc networks. In our geo-regioning approach we will only consider the shape of the signatures given by the relative positions of the multipath components but not the absolute temporal positions. Compared to ToA based techniques, for the geo-regioning approach much more relaxed timing and synchronization accuracy is sufficient. Furthermore, there is no special protocol required for the transmitters to be localized as it is, e.g., for ranging [1]. This makes geo-regioning in particular appropriate for asynchronous networks. Since there are only estimates of the signatures required at the receiver, heterogeneous types of UWB transmitters as, e.g., sensors, tags or communication devices can be localized. Although the performance of such a system can be increased using several receivers at different positions (as it is usual in localization systems [4][5]), only one single antenna receiver is sufficient for geo-regioning. Additionally, geo-regioning is a promising approach for localization in environments where no direct path can be received.

The aim of this paper is to show the principle feasibility of the geo-regioning approach. We will show that the knowledge of the average power delay profiles of the different regions is sufficient to perform the regioning decision with reasonable reliability. This means that average power delay profiles contain enough information to enable proper differentiation between signatures originating from different regions and, at the same time, that there are enough similarities between signatures originating from a single region. It is obvious that the feasibility and performance of the geo-regioning approach depend very much on characteristics of propagation channel and environment. Therefore, a measurement campaign has been performed which provides an appropriate set of data to investigate the geo-regioning approach by means of measured data.

The measurement campaign is described in Section II. In Section III, we introduce a first geo-regioning algorithm which uses full a priori knowledge of the average power delay profiles of the regions. We finally show initial performance results in Section IV and conclude in Section V.

0-7803-9152-7/05/$20.00 © 2005 IEEE

II. Measurements

A. Measurement Setup and Scenario

The measurements considered in this work are explicitly performed to support investigations of geo-regioning. The intention of the measurements is to consider a number of selected regions in a room and to collect a high number of CIRs from each region. The knowledge of exact position of the transmitter inside a region is not required.

A time-domain MIMO measurement setup using correlation method with 4 TX and 3 RX antennas is used. The spacing of the antennas is $d \geq 20$cm. TX and RX array were mounted in a height of 180cm. On the transmitter side 4 pseudo random bit sequence generators are running in parallel. The bit sequences are temporally shifted by at least 250ns to each other. This corresponds to a path length of 75m. We assume that the power of paths with higher length is negligible for our considerations. The TX antenna array was mounted on a two dimensional positioner which itself was placed on a wagon. The postioner allows to move the array in an area of 270mm x 560mm. The wagon was placed in a wide spacing at many positions in the room. We associate to each position of the wagon a certain region (see Fig. 2). The RX array was placed on a tripod at a fixed position in the room. Three parallel channels of a real time sampling scope (Lecroy SDA 6020) are used, sampling at a frequency of 20GHz. The trigger at the scope is not synchronized with the positioner of the TX array. That means that the exact positions of the TX antennas are not known. However, since the array is moved by the positioner when the position of the wagon is fixed, the measured CIRs are located insight the region of the wagon. Since triggering at the scope is done periodically and the speed of the array is approximately constant the measured points have nearly equidistant spacing. The spacing is about 1.7cm and the speed of the positioner is of about 1cm/s. All measurements are performed in a cellar room of building ETF at ETH Zurich, which could be seen as a warehouse-like scenario. The room has a size of about 7.4m x 45m and the height is about 6m. Only one half of the room was used for the measurements. There are many products of various stature and material stored in the room. The room contains many metallic objects as, e.g., large metallic shelves, heating pipes and metal cores but there were hardly any continuously wave blocking objects as, e.g., walls or cabinets, which may be a significant difference to the industrial environment presented in [6]. Fig. 1 shows a picture of the room. Fig. 2 shows a floor plan of the room including some details on the furniture with the positions of the wagon and the position of the receive array. Due to the chosen position of the RX array we have typical LOS regions from Region 1 to 11 and in Region 13 and 14. Typical NLOS region are 16 to 21.

A number of roughly 150 trigger events have been performed for each region. Since each trigger means $4 \cdot 3 = 12$ channel impulse responses this yields a number of $12 \cdot 150 = 1800$ CIRs per region. The wagon was placed at 22 different positions. So, a total number of 39600 CIRs have been collected. This set of data provides the basis for our geo-regioning investigations. As a first step, only single antenna links are considered. Future investigations will take the impact of multiple antenna systems into account.

Fig. 1. Picture of the measurement room

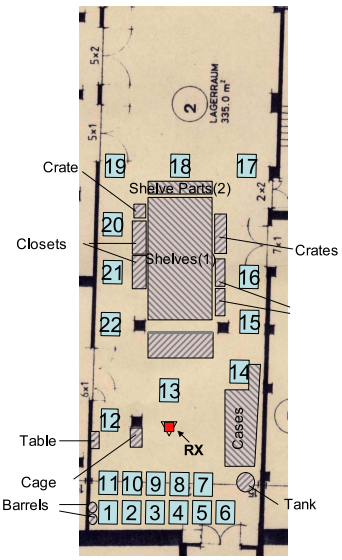

Fig. 2. Positions of RX array and wagon

B. RMS Delay Spread

To get an impression of the measured data we have a look on the cumulative distribution function (CDF) of the RMS delay spread τ_{RMS} which is defined as

$$\tau_{RMS} = \sqrt{\overline{\tau^2} - \overline{\tau}^2}, \tag{1}$$

with

$$\overline{\tau^k} = \frac{\int \tau^k \cdot p(\tau) d\tau}{\int p(\tau) d\tau} \tag{2}$$

and $p(\tau) = |h(\tau)|^2$ the instantaneous power delay profile. this is shown in Fig. 3 for all measured regions. The full range of τ_{RMS} is from about 11ns to 37ns. The NLOS regions 17, 18 and 19 have the largest delay spread whereas the LOS regions which are nearest to the receiver have the

smallest delay spread. These regions have very similar CDFs and the range of τ_{RMS} is only about 5ns. The small range of τ_{RMS} indicates that the signatures in these regions look very similar. We can assume that these regions can easily be distinguished from regions with different τ_{RMS} but can harder be distinguished mutually. Regions 17, 18 and 19 show a high range in τ_{RMS} of up to 14ns. We can assume that the signatures within these regions look quite different and therefore detecting the correct region might be more difficult. In section IV these assumptions are confirmed by simulation results. Note that these considerations assume a signal to noise ratio definition as usually used in communication systems (see Eq. (12)).

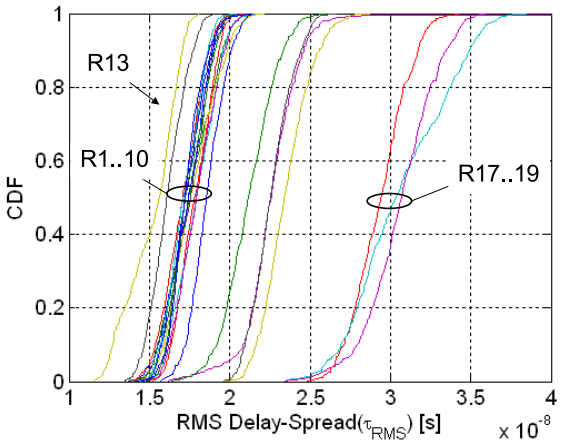

Fig. 3. CDF of RMS delay spread

C. Power Delay Profile and Average Power Delay Profile

In Section III, a geo-regioning algorithm will be proposed which is based on the average power delay profiles (APDP) of the regions. The APDP of a Region A is determined by

$$\text{APDP}_A(k) = \frac{1}{N_A} \sum_{m=1}^{N_A} |h_{A,m}(k)|^2, \qquad (3)$$

where N_A is the number of available measurements of impulse responses or signatures from Region A represented by the sampled series $h_{A,m}(k)$. The m-th PDP of Region A is then $|h_{A,m}(k)|^2, k = 1...K$. In Fig. 4, a section of the PDPs of the LOS Region 3 and the NLOS Region 18 is depicted. In this figure high values are plotted in dark colors and low values in light colors. The index is the number (m) of the measurement and corresponds to a position within the region. Since the absolute temporal position of the CIRs have not been measured, the PDPs are aligned by their maximum values. The LOS nature of Region 3 can be observed by the very strong peak at time 15ns which is clearly the maximum. After that peak, several clusters are visible which may be significant for that region. For the NLOS Region 18 the alignment is much more difficult. Some mistakes in the alignment can be observed, e.g., at indices 37 and 122. At higher indices (> 100) two dominant peaks appear. Many clusters can be observed before and after the maximum peak arrives. In Fig. 5, the APDPs are shown. The receive power of Region 3 is much higher than that of Region 18 which is located farther away from the RX position (see Fig. 2). Also if we neglect the difference in the receive power, the APDP look still very different. In

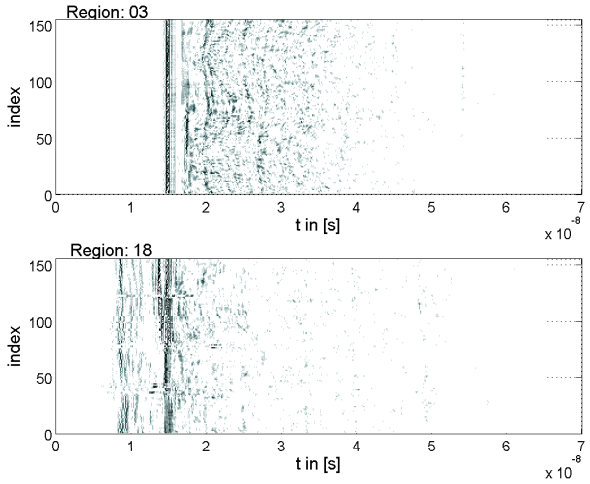

Fig. 4. PDPs of Regions 3 and 18

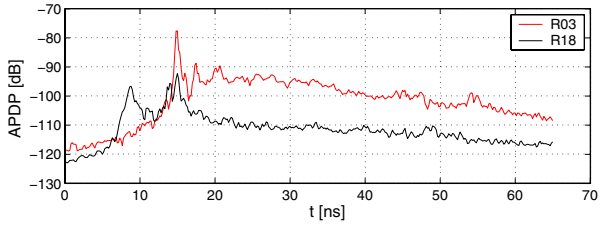

Fig. 5. APDPs of Regions 3 and 18

Fig. 6, the APDPs of two NLOS regions, Region 17 and 19, are shown. Both regions have almost the same distance to the receiver and are located almost symmetrically in the room (see Fig. 2). Although the APDPs look quite similar, significant differences which are indicated by the arrows can be observed. These considerations motivate the algorithm proposed in Section III.

III. A SIMPLE GEO-REGIONING ALGORITHM

In this paper, we consider the geo-regioning application where a rough localization of the transmitter is requested as described in Section I. This means that a transmitter has to be localized by associating its position to a region just by means of its signature. The main goal here is to propose a simple algorithm proving the principle feasibility of such a geo-regioning approach.

We assume that the average power delay profiles (APDP) of all regions are a priori known at the receiver. To derive a simple algorithm which detects the region by the received

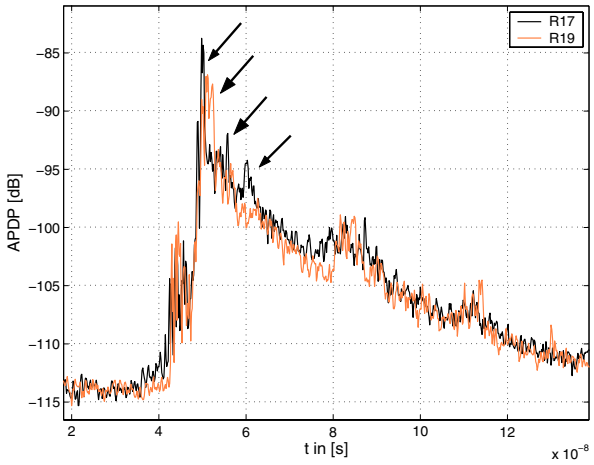

Fig. 6. APDPs of Regions 17 and 19

signature we make the following simplifying assumption: Each signature $x(k)$ with $k = 1...K$ is an outcome from a random process that generates statistically independent Gaussian variables. The Gaussian distribution is zero mean and the variance at index k depends on the region where the signature originates from and is set to the corresponding APDP value:

$$\sigma^2(k) := \text{APDP}(k) \tag{4}$$

So, the probability density of $x(k)$ which is originating from Region A is $\mathcal{N}(0, \sigma_A^2(k))$:

$$p(x(k)|A) = \frac{1}{\sqrt{2\pi}\sigma_A(k)} \cdot \exp\left(-\frac{x^2(k)}{2\sigma_A^2}\right) \tag{5}$$

A maximum likelihood (ML) estimator that considers all possible regions $\mathcal{A}$ maximizes the probability density

$$\max_{\mathcal{A}} p(\vec{x}|\mathcal{A}), \tag{6}$$

with $\vec{x}[k] = x(k), k = 1...K$. The ML estimator deciding between two regions A and B is:

$$p(\vec{x}|A) \underset{B}{\overset{A}{\gtrless}} p(\vec{x}|B), \tag{7}$$

Since the samples $x(k)$ are assumed to be statistically independent the log-likelihood can be derived:

$$\prod_{k=1}^{K} p(x(k)|A) \underset{B}{\overset{A}{\gtrless}} \prod_{k=1}^{K} p(x(k)|B) \tag{8}$$

$$\Leftrightarrow \sum_{k=1}^{K} \ln\left(\frac{1}{\sqrt{2\pi}\sigma_A(k)} \cdot \exp\left(-\frac{x^2(k)}{2\sigma_A^2}\right)\right) \underset{B}{\overset{A}{\gtrless}} \sum_{k=1}^{K} \ln\left(\frac{1}{\sqrt{2\pi}\sigma_B(k)} \cdot \exp\left(-\frac{x^2(k)}{2\sigma_B^2}\right)\right)$$

$$\Leftrightarrow \sum_{k=1}^{K} x^2(k) \frac{\sigma_A^2(k) - \sigma_B^2(k)}{\sigma_A^2(k)\sigma_B^2(k)} \underset{B}{\overset{A}{\gtrless}} \sum_{k=1}^{K} \ln \frac{\sigma_A^2(k)}{\sigma_B^2(k)} \tag{9}$$

IV. Performance Results

A. Performance Measure and Simulations

In this section the performance of the algorithm is shown by means of simulations running with the measured data. As a performance measure we use the pairwise error probability when deciding between two regions. We assume that we have received a noisy estimate $v(k), k = 1...K$ of the signature $x(k)$, where $n(k)$ denotes an additive zero mean Gaussian noise component with variance σ_n^2:

$$v(k) = x(k) + n(k) \tag{10}$$

Hence, $v(k)$ is the sum of two Gaussian distributed random variables. If we assume $x(k)$ originating from Region A, the probability density function of $v(k)$ is $\mathcal{N}(0, \sigma_A^2(k) + \sigma_n^2)$. With $\sigma_{A'}^2(k) = \sigma_A^2(k) + \sigma_n^2$ the ML estimator from (8) can be written as:

$$\sum_{k=1}^{K} x^2(k) \frac{\sigma_{A'}^2(k) - \sigma_{B'}^2(k)}{\sigma_{A'}^2(k)\sigma_{B'}^2(k)} \underset{B}{\overset{A}{\gtrless}} \sum_{k=1}^{K} \ln \frac{\sigma_{A'}^2(k)}{\sigma_{B'}^2(k)} \tag{11}$$

As performance measure the pairwise error probability, $P_2(e)$, is plotted over receive SNR. 150 signatures from one region and 150 from another region are taken from the measurements and added with white Gaussian noise with variance σ_n^2. The detector of (11) is applied and its error performance is evaluated. The SNR is defined by the mean received power per signature over the noise power:

$$\text{SNR} = \frac{1}{\sigma_n^2} \cdot \frac{1}{N_A + N_B} \sum_{m=1}^{N_A+N_B} \sum_{k=1}^{K} |h_m(k)|^2 \tag{12}$$

B. Scalar Error Probability and Number of Taps

To get a better insight into the algorithm, we investigate the simple case of one single tap ($K = 1$). Then, the two hypotheses A and B correspond to two Gaussian distributions with zero mean and variances $\sigma_{A'}^2$ and $\sigma_{B'}^2$. If the error probability that an outcome v of Region B is detected as an outcome from Region A is written as $P_e(A|B)$, the total error probability is:

$$P_2(e) = \frac{1}{2}P_e(A|B) + \frac{1}{2}P_e(B|A) \tag{13}$$

It can be shown that $P_2(e)$ depends only on the ratio α of the two variances

$$\alpha := \max\left\{\frac{\sigma_{A'}^2}{\sigma_{B'}^2}, \frac{\sigma_{B'}^2}{\sigma_{A'}^2}\right\} \tag{14}$$

and is given by:

$$P_2(e) = \frac{1}{2} + \frac{1}{2}\left[\text{erf}\left(\sqrt{\frac{\alpha \cdot \ln \alpha}{2(\alpha - 1)}}\right) - \text{erf}\left(\sqrt{\frac{\ln \alpha}{2(\alpha - 1)}}\right)\right] \tag{15}$$

For $\alpha = 10$ the error probability gets $P_2(e) = 0.25$ and for $\alpha = 100$ it is $P_2(e) = 0.1$. Since for the most region pairs the maximum ratio is below 10 we can expect that a high number of taps is required to make a reliable decision. Fig. 7 shows a simulation result for the very similar regions 17 and 19

from Fig. 6. The K taps with maximum ratio α are selected for this simulation with $K = 1, 30, 60, 300, 600$. The best performance is achieved with $K = 600$ taps. Decreasing K decreases the performance and an error floor can be observed. As expected $K = 1$ is not useful and yields $P_2(e) > 0.1$ in the considered SNR range. The performance curve shows first an improvement with increasing SNR and then it decreases back to $P_2(e) = 0.5$ at SNR $\geq$ 40dB. The reason for this behavior is that the index k that maximizes α depends on the SNR. In the lower SNR region the ratio α is maximized at an index k_1 where both APDP values are high. For this index the performance improves with increasing SNR. At higher SNR values ($\geq$ 40dB), however, the ratio α is maximized at an index $k_2 \neq k_1$ where both APDP values are very low. For this index our Gaussian model matches not the real distribution. For comparison the dotted line shows the performance with a Gaussian distributed tap generated by simulations. Here the performance increases monotonously with SNR.

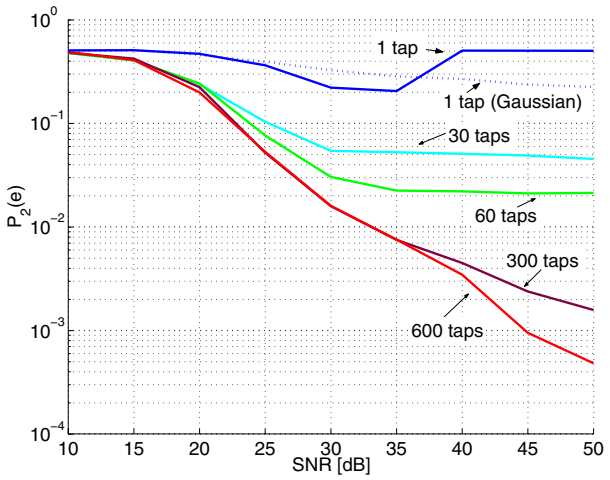

Fig. 7. Pairwise error probabilities for Regions 17 & 19 for various number of taps

C. Performance for Various Regions

In Fig. 8, the pairwise error probabilities for some exemplary region pairs are shown. Regions 1 and 2 are LOS regions where the signatures have many similarities with the ones from Region 3. The region pair 2&3 shows poorest performance. This could be expected since both regions are located very close together. Some of the measured positions in R2 were located only a few cm apart from some positions of R3. The pair 3&17 shows best performance because R3 is strong LOS and R17 strong NLOS. Since these regions could simply be distinguished by the received energy we have normalized the received energy for both regions and simulated the performance again (*R3&17 normalized*). Although the performance decreases by about 10dB both regions can still be detected very well. Finally, for comparison the performance of the pair 17&19 is shown. We conclude that almost all region pairs achieve $P_2(e) \leq 10^{-2}$ for SNR $<$ 35dB and hence can be separated at reasonable receive SNR. Note that for CIR estimation we can expect 10dB to 15dB more SNR than for data detection.

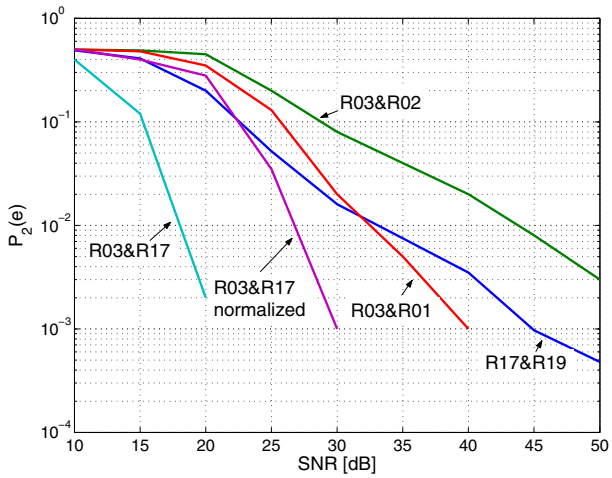

Fig. 8. Pairwise error probabilities for various region pairs

V. Conclusions

We have introduced the principle of geo-regioning and proposed a first algorithm. The principle feasibility of geo-regioning was shown by means of measured data . In case of very critical regions the algorithm requires a huge number of taps (> 60) to achieve error probabilities below 10^{-2}. However, also in this case reasonable performance could be achieved. Future work will concern improvement and complexity reduction of the geo-regioning algorithm, derivation of theoretical performance bounds and the impact of using multiple antennas at TX and RX, respectively.

VI. Acknowledgement

The authors would like to thank all partners of the PULSERS project (www.pulsers.net), that was partially funded by the European Commission and the Swiss Federal Office for Education and Science, for their contributions and constructive discussions.

References

[1] Joon-Yong Lee and Robert A. Scholtz. Ranging in a dense multipath environment using an UWB radio link. In *IEEE Journal on Selected Areas in Communications, Vol. 20, No.9*, pages 1677–1683, December 2002.

[2] B. Denis, J. Keignart, and N. Daniele. Impact of NLOS propagation upon ranging precision in UWB systems. In *IEEE Conference on Ultra Wideband Systems and Technologies*, pages 379 – 383, November 2003.

[3] C. Prettie, D. Cheung, and L. Ruschand M. Ho. Spatial correlation of UWB signals in a home environment. In *IEEE Ultra Wideband Systems and Technologies*, pages 65 – 69, May 2002.

[4] S. J. Ingram, D. Harmer, and M. Quinlan. Ultra wideband indoor positioning systems and their use in emergencies. In *Position Location and Navigation Symposium*, pages 706 – 715, April 2004.

[5] D. Niculescu. Positioning in ad hoc sensor networks. In *Network, IEEE*, pages 24 – 29, July/August 2004.

[6] J. Karedal, S. Wyne, P. Almers, F. Tufvesson, and A. Molisch. UWB channel measurements in an industrial environment. In *IEEE Globecom*, 2004.